Acta Crystallographica Section D
Biological Crystallography
ISSN 0907-4449

Structure of the ribosomal protein L1–mRNA complex at 2.1 Å resolution: common features of crystal packing of L1–RNA complexes

S. Tishchenko,[a] E. Nikonova,[a] A. Nikulin,[a] N. Nevskaya,[a] S. Volchkov,[b] W. Piendl,[c] M. Garber[a] and S. Nikonov[a]*

[a]Institute of Protein Research, Russian Academy of Sciences, 142290 Pushchino, Moscow Region, Russia, [b]Institute of Cell Biology, Russian Academy of Sciences, 142290 Pushchino, Moscow Region, Russia, and [c]Biocenter, Division of Medical Biochemistry, Innsbruck Medical University, Fritz-Pregl-Strasse 3, 6020 Innsbruck, Austria

Correspondence e-mail: nikonov@vega.protres.ru

Received 7 August 2006
Accepted 9 October 2006

PDB Reference: L1–mRNA, 2hw8, r2hw8sf.

The crystal structure of a hybrid complex between the bacterial ribosomal protein L1 from *Thermus thermophilus* and a *Methanococcus vannielii* mRNA fragment containing an L1-binding site was determined at 2.1 Å resolution. It was found that all polar atoms involved in conserved protein–RNA hydrogen bonds have high values of density in the electron-density map and that their hydrogen-bonding capacity is fully realised through interactions with protein atoms, water molecules and K^+ ions. Intermolecular contacts were thoroughly analyzed in the present crystals and in crystals of previously determined L1–RNA complexes. It was shown that extension of the RNA helices providing canonical helix stacking between open–open or open–closed ends of RNA fragments is a common feature of these and all known crystals of complexes between ribosomal proteins and RNAs. In addition, the overwhelming majority of complexes between ribosomal proteins and RNA molecules display crystal contacts formed by the central parts of the RNA fragments. These contacts are often very extensive and strong and it is proposed that they are formed in the saturated solution prior to crystal formation.

1. Introduction

L1 is one of the largest ribosomal proteins located on the side protuberance opposite the L7/L12 stalk of the 50S ribosomal subunit. In bacteria and archaea, protein L1 is able to regulate gene expression by binding to its own mRNA, thereby acting as a translational repressor (Gourse *et al.*, 1986; Mayer *et al.*, 1998; Kraft *et al.*, 1999). L1 proteins from mesophilic and thermophilic bacteria and archaea bind to the specific site on 23S rRNA with at least a fivefold to tenfold higher affinity than to their regulatory binding site on their mRNAs (Köhrer *et al.*, 1998). This difference fits the requirements of the classical regulation of ribosomal protein synthesis (feedback inhibition) based on direct competition between two binding sites. Structural studies and comparison of L1–rRNA and L1–mRNA complexes should be useful in elucidating how proteins and RNA molecules modulate their affinity for each other.

Ribosomal protein L1 is structurally and functionally interchangeable within the ribosomes from different species (Gourse *et al.*, 1981; Baier *et al.*, 1989). Thus, L1 from the archaeon *Methanococcus vannielii* (MvaL1) can functionally replace *Escherichia coli* L1 (EcoL1) in the *E. coli* ribosome (Baier *et al.*, 1990). It has also been shown that EcoL1 can inhibit *in vitro* translation of MvaL1 polycistronic mRNA and conversely that MvaL1 can inhibit synthesis of *E. coli* proteins L11 and L1 (Hanner *et al.*, 1994). This indicates that the RNA-

binding sites on the L1 proteins and the protein-binding sites on the corresponding RNA molecules are structurally highly conserved; therefore, hybrid L1–RNA complexes are suitable for structural studies. For structural studies, we used hybrid complexes between ribosomal proteins and specific RNA fragments from different organisms, because sometimes such complexes are better for crystallization than homologous nonhybrid complexes (Garber *et al.*, 2002).

Firstly, crystals of L1–RNA complexes suitable for X-ray investigations were obtained by our group for the hybrid complex between *Sulfolobus acidocaldarius* L1 (SacL1) and a specific fragment of 23S rRNA from *Thermus thermophilus*. The structure of the complex was determined at 2.65 Å resolution (Nikulin *et al.*, 2003). We subsequently succeeded in the crystallization of two regulatory L1–mRNA complexes. The structures have been solved for a homologous L1–mRNA complex from *Methanococcus jannashii* at 3.4 Å resolution (Nevskaya *et al.*, 2005) and for a hybrid complex between the bacterial protein L1 from *T. thermophilus* (TthL1) and a fragment of mRNA from the archaeon *M. vannielii* ($mRNA_{MvaL1}$) at 2.6 Å resolution (Nevskaya *et al.*, 2006). Analysis of these structures revealed common and distinctive features of the L1–rRNA and L1–mRNA interactions. Nevertheless, high-resolution structures were needed to localize water molecules and ions and to understand in detail how L1 regulates its own synthesis.

Here, we describe the crystallization trials carried out to obtain the best crystals of an L1–mRNA complex and present the 2.1 Å resolution crystal structure of a hybrid complex between the bacterial protein L1 from *T. thermophilus* and a 36 nt fragment of mRNA for L1 ($mRNA_{MvaL1}$) from the archaeon *M. vannielii*. A detailed analysis of crystal contacts in the present and other L1–RNA complexes lets us reveal some common features of ribosomal protein–RNA crystal packing which are of interest for crystallization strategy.

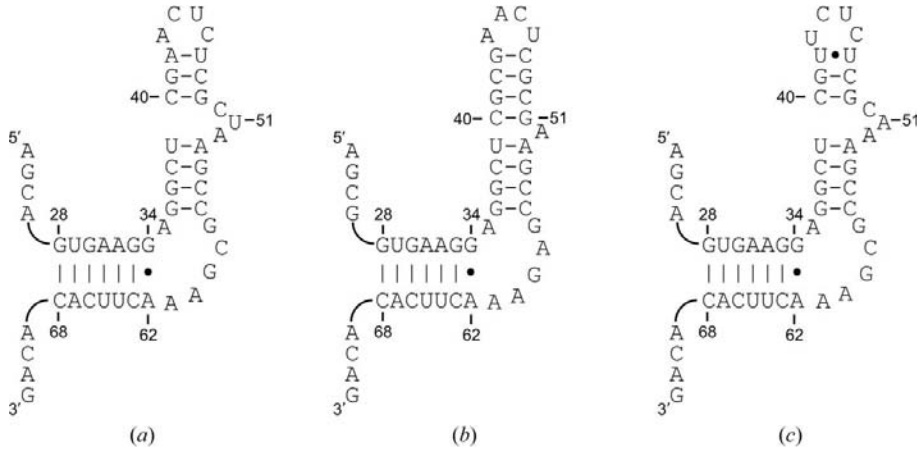

Figure 1
Fragments of (*a*) *M. vannielii*, (*b*) *M. jannaschii* and (*c*) *M. thermolithotrophicus* mRNAs containing regulatory L1-binding sites.

2. Materials and methods

2.1. Choice of mRNA fragments

The L1-binding site on $mRNA_{MvaL1}$ is located about 30 nucleotides downstream of the ATG start codon and includes an asymmetric loop flanked by two helices. Comparison of the L1-binding sites on *M. vannielii* $mRNA_{L1}$ and the closely related *M. jannashii* and *M. thermolithotrophicus* mRNAs (Fig. 1) shows that the sequences of the helices containing nucleotides +28 to +34 and +62 to +68 are identical in the three species, whereas the sequences of the upper part of the stem-loop structure (comprising nucleotides +40 to +51) are poorly conserved between these species. Thus, it is a reasonable assumption that this stem-loop structure is not essential for L1 binding. Nevertheless, the 30 nt fragment of *M. vannielii* $mRNA_{L1}$ containing nucleotides +28 to +38 and +54 to +68 and closed with the tetraloop UUCG (Fig. 2*a*) does not exhibit any specific affinity for protein L1, whereas the same fragment with four additional base pairs at the open end of the helix binds L1 with virtually the same affinity as a 250 nt $mRNA_{MvaL1}$ fragment (data not shown). The complex of TthL1 with such a 38 nt mRNA fragment was crystallized and the crystals obtained diffracted to 2.6 Å resolution (Nevskaya *et al.*, 2006). To further improve the quality of the L1–mRNA crystals, we varied the length and content of both of the helices flanking the asymmetric mRNA loop. We also tried using mRNA fragments with unpaired nucleotides since they can affect the crystal packing (Garber *et al.*, 2002). Finally, various *M. vannielii* and *M. jannashii* $mRNA_{L1}$-specific fragments of 36–49 nt length were prepared by *in vitro* transcription (Fig. 2) and tested for TthL1- and MjaL1-binding activity using filter binding assays. The affinity of TthL1 and MjaL1 proteins for these rather short mRNA fragments was virtually the same as their affinity for the long (250 nt) fragment of $mRNA_{MvaL1}$. The RNA transcripts were purified by gel electrophoresis under denaturing conditions to a homogenous state and used to obtain L1–mRNA complexes.

All obtained mRNA fragments formed stable complexes with the L1 proteins from the bacterium *T. thermophilus* and the archaea *M. jannashii*, *M. thermolithotrophicus* and *S. acidocaldarius*, but crystals were only obtained for complexes containing TthL1 or MjaL1.

2.2. Crystallization

RNA fragments prepared for crystallization trials were dissolved at a concentration of 5–7 mg ml^{-1} and renatured by heating at 333 K for 10 min. Solutions of RNA and TthL1 or MjaL1 were mixed in equimolar amounts and $MgCl_2$ was added to 1.5 m*M* final concentration.

Crystals were grown by the hanging-drop vapour-diffusion method. Crystallization conditions for the MjaL1–$mRNA_{MjaL1}$

and TthL1–mRNA$_{MvaL1}$ complexes were rather similar and used PEG 8–10K as a precipitant in sodium cacodylate buffer pH 5.5–7.0. 0.5% glycerol and 0.2 m*M* mercury compounds were used as additives for TthL1–mRNA complexes and 0.7% 2-methyl-2,4-pentanediol was used for MjaL1–mRNA complexes. Crystals of TthL1–mRNA complexes were grown at 277 K, whereas crystals of MjaL1–mRNA complexes were grown at both 277 K and at room temperature.

2.3. Data collection and structure determination

The best crystals were obtained for the complex of TthL1 with the 36 nt fragment of mRNA$_{MvaL1}$ (Fig. 2*d*). They diffracted to 2.1 Å resolution and belong to space group $P6_522$. Diffraction data were collected at EMBL beamline BW7B equipped with a MAR345 image-plate detector at the DORIS storage ring, DESY (Hamburg, Germany). Owing to the large unit-cell parameters of the crystal (Table 1), an oscillation angle of 0.25° was used. Data were processed and merged with the *XDS* program suite (Kabsch, 2001).

The structure was solved by molecular replacement with *AMoRe* (Navaza, 1994) using the partly modified 2.6 Å resolution structure of TthL1 in complex with a 38 nt fragment of mRNA$_{MvaL1}$ (PDB code 1zho) as a search model. A clear solution with a correlation coefficient of 0.725 and an *R* factor of 0.359 was obtained for diffraction data between 15 and 3.0 Å.

The model was subjected to several rounds of computational refinement and map calculation with *CNS* (Brünger *et al.*, 1998) and manual model inspection and modification with *O* (Jones *et al.*, 1991). To overcome the model bias, we used composite OMIT cross-validated σ_A-weighted maps as implemented in *CNS*. A free *R* factor, calculated from 5% of reflections set aside at the outset, was used to monitor the progress of refinement. The initial overall *B* factor was finally replaced by restrained individual atomic *B* factors. When the *R* factor reached 25.7%, water molecules were placed into 3σ peaks of $F_o - F_c$ maps when they were within a suitable hydrogen-bonding distance of the existing model. After refinement, water molecules whose positions were not supported by electron density at 1σ contouring in a σ_A-weighted $2F_o - F_c$ map were deleted.

The final model, refined to an *R* factor of 21.2% (R_{free} = 24.7%) at 2.1 Å resolution, includes 228 amino acids, 36 nucleotides, 163 water molecules, a 2,4-butanediol molecule, Mg^{2+} and K^+ ions. Data and refinement statistics are

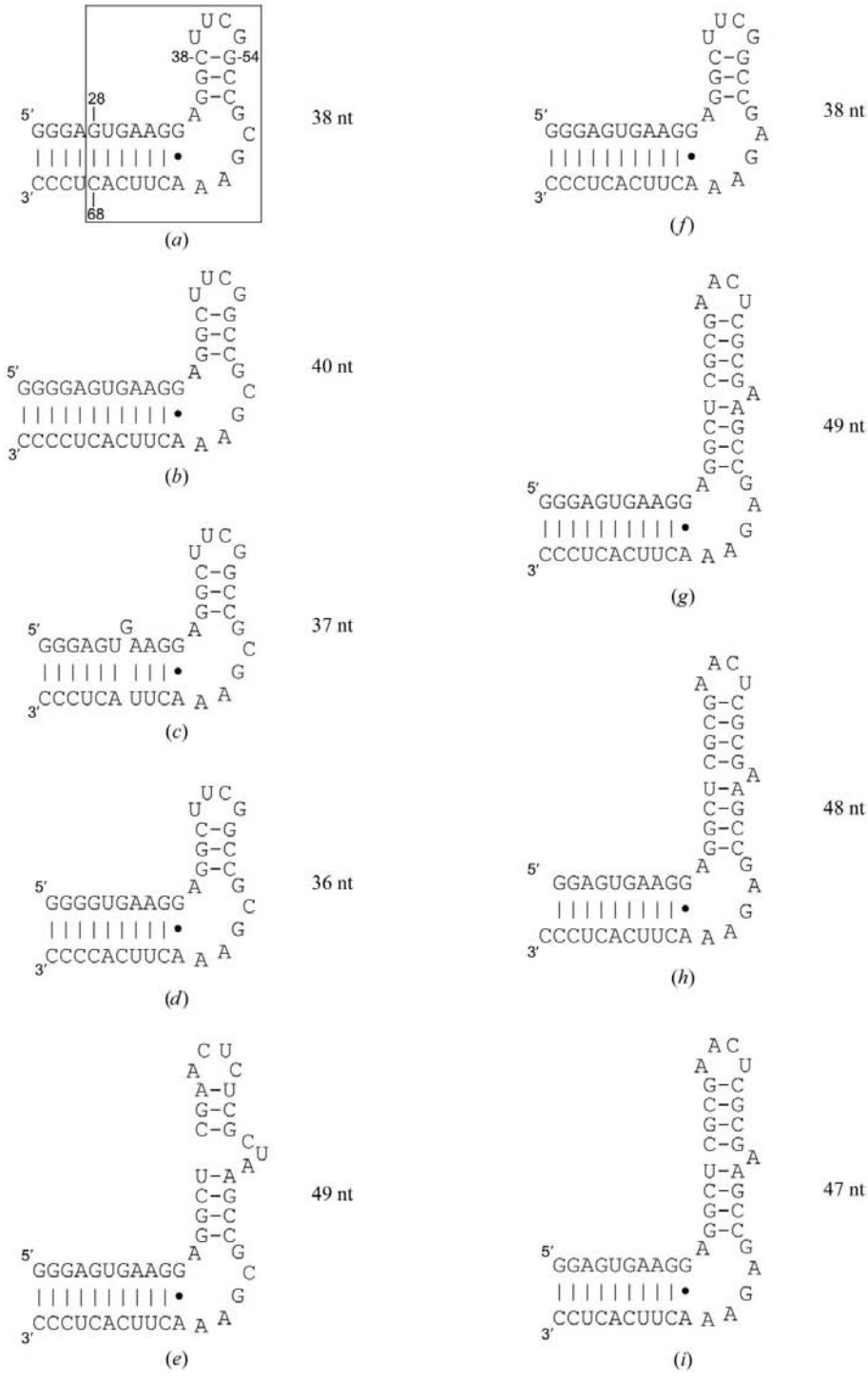

Figure 2
Fragments of mRNA from *M. vannielii* (*a*–*e*) and *M. jannaschii* (*f*–*i*) used to obtain L1–mRNA complexes. The length and content of both helices flanking the asymmetric loop were varied. The 30 nt fragment is boxed in (*a*).

summarized in Table 1. Fig. 3 provides an example of the quality of the final $2F_o - F_c$ electron-density map.

3. Results and discussion

3.1. Overall description of the structure

Components of the TthL1–mRNA$_{MvaL1}$ complex and a stereoview of its structure are shown in Fig. 4. The overall three-dimensional structure of TthL1 (Fig. 4*b*) is closely related to that found in the 2.6 Å resolution structure of the homologous TthL1–mRNA complex (Nevskaya *et al.*, 2006). The two complexes crystallized in different space groups; nevertheless, both structures show that in complex with RNA TthL1 is in the open conformation, in contrast to the closed conformation found previously for the isolated TthL1 protein (Nikonov *et al.*, 1996). In the present complex, the mRNA fragment is two nucleotides shorter than the fragment of mRNA in the previously determined homologous structure. This difference results in a change in crystal packing and symmetry.

3.2. Structure of TthL1

The ribosomal protein TthL1 folds into two domains, with the N- and C-termini close to each other in domain I. As a result, the hinge region between the domains consists of two connections. Domain I contains a four-stranded antiparallel β-sheet (β_1, β_8, β_9, β_{10}) flanked by two α-helices (α_2, α_7) on one side and exposed on the other. The N-terminal helix is quite separated from the globular part of domain I and is associated with it by hydrophobic interactions with helix α_2 and strand β_{10} and a hydrogen bond between Lys13 and Glu31. Two strands (β_2, β_7), which are distant from the main β-sheet of domain I, connect two domains and form the hinge region. Domain II has an overall Rossmann-fold topology and contains two α-helices on each side of a four-stranded parallel β-sheet. The recently determined 2.6 Å resolution structure of the homologous complex contains four similar but non-identical copies of TthL1-mRNA (Nevskaya *et al.*, 2006). In these copies, the TthL1 domain structures are essentially the same, but the mutual orientation of the domains is somewhat different. The structures of two molecules with the maximum opening of the interdomain cavity are very close to that of TthL1 in the present complex. They were superimposed using the least-squares option of *O* with an r.m.s. deviation of 0.5 Å for all C^{α} atoms.

3.3. Structure of the mRNA$_{MvaL1}$ fragment

The fragment of *M. vannielii* mRNA used to obtain the present complex includes nucleotides 28–38 and 54–68 (Fig. 2*d*). One end of the fragment is capped with the tetraloop UUCG, while the other is elongated by three additional Watson–Crick G–C base pairs. The structure of the fragment involves long (helix 1) and short (helix 2) regular double helices practically perpendicular to each other (Figs. 2*d* and 4*c*). These helices are separated by the asymmetric loop, which contains the noncanonical *trans* Hoogsteen/sugar-edge base pair A62·G34 (Leontis & Westhof, 2001). The closing tetraloop UUCG is found to adopt a conformation similar to that described earlier (Ennifar *et al.*, 2000). The chain G25–C38

Table 1
Data-collection and refinement statistics.

Values in parentheses are for the highest resolution shell.

Data collection	
Wavelength (Å)	0.843
Resolution (Å)	25–2.1
Space group	$P6_522$
Unit-cell parameters	
a (Å)	67.87
b (Å)	67.87
c (Å)	340.47
α (°)	90
β (°)	90
γ (°)	120
No. of reflections	176789 (27541)
No. of unique reflections	28370 (4317)
Averaged redundancy	6.2 (6.4)
Completeness (%)	99.3 (97.1)
$R_{sym}(I)$ (%)	7.5 (34.2)
$I/\sigma(I)$	14.9 (4.3)
Refinement	
Resolution (Å)	25–2.1 (2.22–2.1)
No. of protein atoms	1742
No. of nucleic acid atoms	774
No. of water molecules	163
No. of reflections in refinement	28370
No. of reflections in test set	1382
R factor (%)	21.2 (31.0)
R_{free} (%)	24.7 (34.7)
Average overall B factor (Å^2)	38.2
R.m.s. deviation from ideal geometry	
Bond lengths (Å)	0.009
Bond angles (°)	1.50
Improper angles (°)	1.57
Dihedral angles (°)	22.5
Ramachandran plot regions (%)	
Most favoured	88.4
Additionally allowed	11.6
PDB code	2hw8

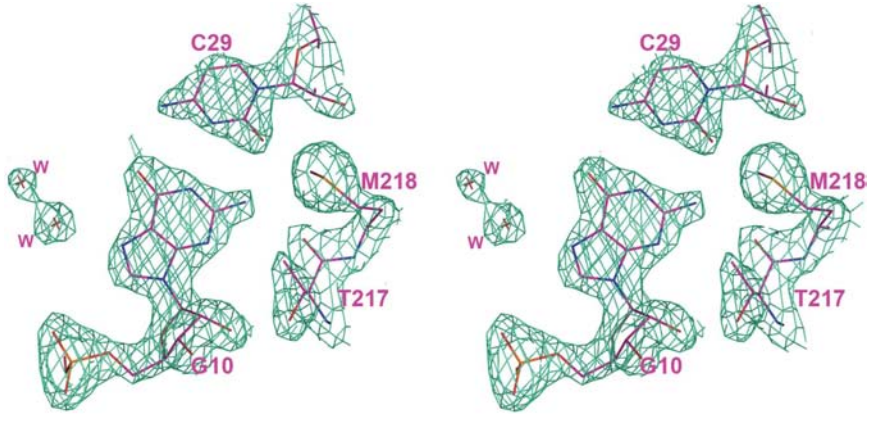

Figure 3
Stereoview of a fragment of the final $2F_o - F_c$ electron-density map contoured at 2.0σ.

bends sharply at position G36 and the ribose moieties of A35 and G36 are brought together approximately perpendicular to each other. An extensive network of hydrogen bonds, which involves many base atoms, stabilizes this turn. Nucleotides belonging to the junction of the two RNA helices are highly conserved and form a unique structure constrained by local and long-distance interactions. The surface of the helix 1 of the mRNA fragment is complementary to the surface of the β-sheet of domain I.

3.4. mRNA–TthL1 interactions

Upon complex formation, 1373 Å^2 of RNA surface and 1288 Å^2 of protein surface are buried. The ribosomal protein TthL1 only binds mRNA through the amino-acid residues of domain I. Residues of the β-sheet and adjacent β–β loops of the protein interact with the conserved junction region and helix 1 of the mRNA. Practically all these amino-acid residues are aligned along the shallow groove of the mRNA helix 1. The N-terminal helix of TthL1 mainly interacts with the backbone of the closing tetraloop and additional base pairs at the open end of the RNA fragment. The outside of helix 2 and the asymmetric loop of the RNA do not contact the protein. The RNA–protein complex is stabilized by 32 hydrogen bonds, stacking interactions of Phe37 and His172 with the ribose-phosphate backbone of mRNA and approximately 170 van der Waals contacts. The strongly conserved Glu42 and G33 form the shortest hydrogen bond.

We have previously proposed that conserved hydrogen bonds inaccessible to the solvent play a key role in RNA–

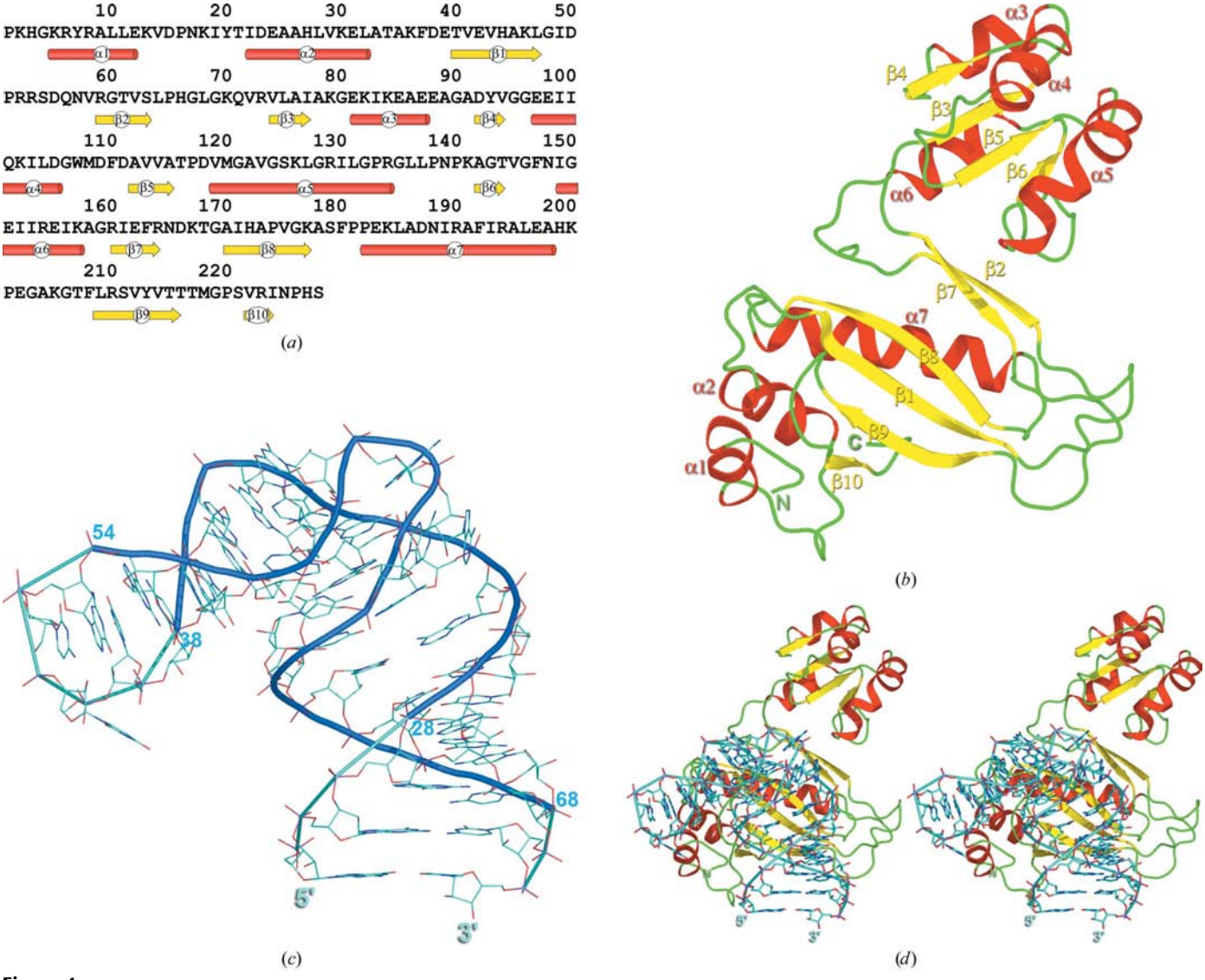

Figure 4
Components of the TthL1–36 nt mRNA complex. (*a*) Amino-acid sequence of the TthL1 protein. α-Helices are shown as red cylinders and β-strands as yellow arrows. (*b*) Ribbon diagram of TthL1 from the present complex; α-helices (red) and β-strands (yellow) are numbered. (*c*) Three-dimensional structure of the mRNA molecule. The P-trace of the closing tetraloop and three additional base pairs introduced into the mRNA fragment to facilitate the crystallization of the complex are shown in thin lines. (*d*) Stereoview of the TthL1–mRNA complex. The protein is shown in red (α-helices), yellow (β-strands) and green (loops) and the mRNA phosphate trace is shown in cyan.

protein recognition and binding (Nevskaya *et al.*, 2004; Gongadze *et al.*, 2005). The TthL1–mRNA complex contains five such bonds. The atoms involved in these hydrogen bonds have high electron density (more than 3σ) and form the maximum possible number of hydrogen bonds through interactions with protein atoms, water molecules and K^+ ions. This should play a determining role in the formation and function of protein–RNA complexes (Lim & Garber, 2005).

More than ten water molecules involved in intermolecular hydrogen bonds are found in the protein–RNA interface. Most of them are grouped on two edges of the contact area between the ribose-phosphate backbone of G30–G33 and strand β7 and between the ribose-phosphate backbone of G37–U39 and the N-terminal α-helix of L1. One water molecule and K^+ ion inaccessible to the solvent are located inside the contact area. This water molecule is involved in three RNA–protein hydrogen bonds, while the positively charged potassium ion is coordinated by RNA and protein groups, with six ligands in the first coordination sphere.

The number of van der Waals contacts between TthL1 and mRNA is approximately five times greater than the number of intermolecular hydrogen bonds. However, the energy of a hydrogen bond strongly exceeds (by about 1.0–1.5 orders of magnitude) the energy of other non-covalent interactions and therefore the role of hydrogen bonds prevails in the L1–mRNA interactions. Nevertheless, an important role in L1–RNA interactions belongs to the strongly conserved Phe37, the ring of which is stacked with the ribose ring of A35 and keeps solvent molecules from entering into the RNA–protein interface. Loop α2–β1 containing Phe37 is displaced in the RNA–protein complex from its position in free TthL1 by about 5 Å and is stabilized by a short (2.62 Å) hydrogen bond between the main-chain N—H group of Lys36 and atom O1P of G37.

3.5. Crystal packing of various L1–RNA complexes

In principle, three types of contacts are possible between adjacent protein–RNA complexes in a crystal: RNA–RNA, protein–protein and RNA–protein contacts. These contacts depend on the shapes of the protein and the RNA and are formed by different parts of these molecules. To design protein–RNA complexes that are optimal for crystallization, it is desirable to obtain some details of their crystal formation. We have determined four crystal structures of L1–RNA complexes from different organisms. Two complexes, TthL1–36 nt mRNA and TthL1–38 nt mRNA, have only a small difference in the mRNA length; nevertheless, the crystals of these complexes have different packing of molecules and thus different diffraction abilities.

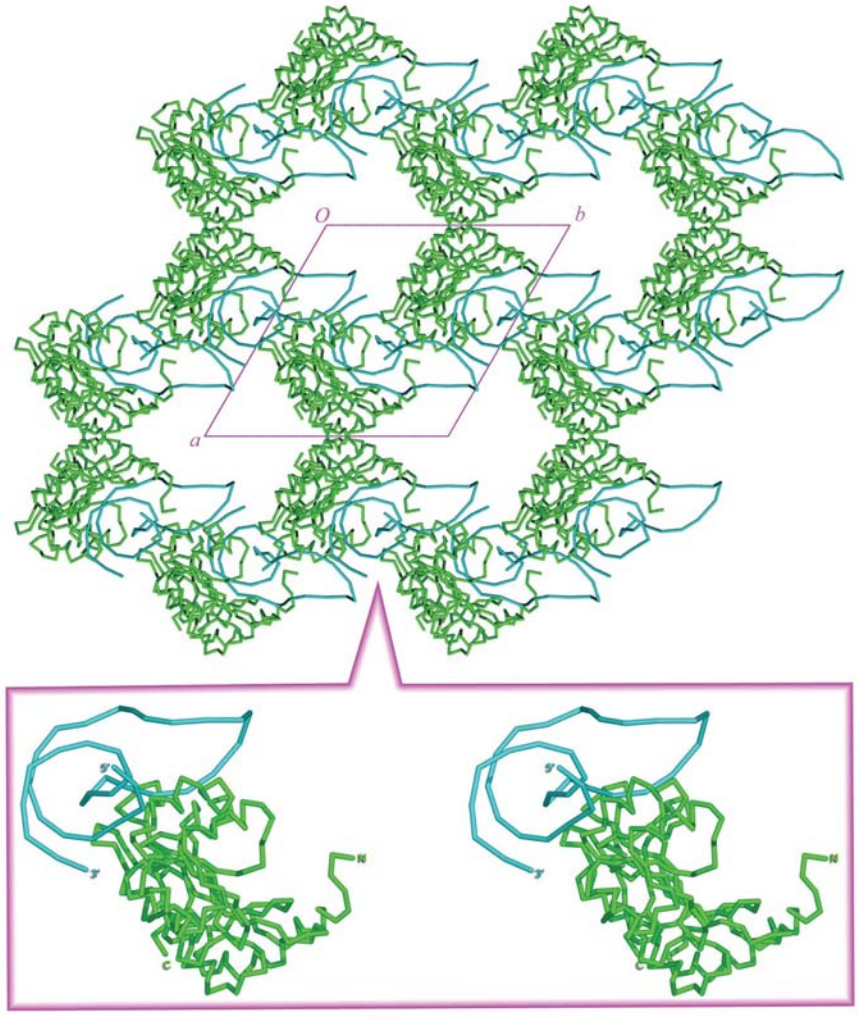

Figure 5
Packing of complexes in a layer of the TthL1–36 nt mRNA crystal. A stereoview of RNA–protein contact between adjacent complexes is shown in close-up.

3.5.1. The TthL1–36 nt mRNA complex crystal. In this crystal, the protein–RNA contact is the strongest and most extensive (Fig. 5). In mRNA, the contact region is formed by the 5′ end and the asymmetric loop. In the protein, it comprises the interdomain region including loop β1–β2 of domain I and the bent helix α5 with the adjacent loop α5–β6 of domain II. Such RNA–protein contacts produce infinite zigzag rows, which are perpendicular to the *c* axis of the crystal and have a bending angle of 120°.

Protein–protein contacts are realised between rows interacting with each other through bent parts. These interactions produce layers perpendicular to the *c* axis of the crystal. Such protein–protein contacts are symmetric and involve the interdomain region (loops β8–α7 and β2–β3) of TthL1.

Adjacent complexes in the row are related by a crystallographic twofold screw axis parallel to the *b* axis of the unit cell. As a result, the open ends of the helices of adjacent mRNA fragments are antiparallel

to each other and are displaced by $b/2$ along the b axis. RNA–RNA contacts are formed between adjacent layers through interaction of the open ends of the mRNA helices (Fig. 6*a*). The stacking between terminal canonical G–C base pairs results in the formation of helices of double length. The distances between neighbouring P atoms of the adjacent complexes are very close to those of a standard A-helix. The shallow groove of such an extended helix is practically unbroken, whereas the deep groove widens at the place of the contact. Interacting complexes are related by a dual axis parallel to the plane of base pairs and perpendicular to hydrogen bonds between them.

3.5.2. The TthL1–38 nt mRNA complex crystal. TthL1 in complex with the 38 nt fragment of mRNA crystallized in space group $P2_1$ (Nevskaya *et al.*, 2006). In this complex, helix 1 of mRNA contains an additional canonical A–U base pair compared with the present complex (Fig. 2*a*). Protein–RNA and RNA–RNA contacts are preserved in the crystals of both the TthL1–mRNA complexes. Nevertheless, the additional base pairs in the complexes, contacting each other through the open ends of mRNA fragments, induce their mutual rotation by about 90° (Fig. 6*b*). This increases the interlayer distances and leads to rearrangement of the complexes in the layers. In this case, protein–protein contacts between zigzag rows are realised through the regions containing the C-terminal ends of symmetry-related proteins.

3.5.3. The MjaL1–49 nt mRNA complex crystal. The 49 nt mRNA fragment used to form the MjaL1–mRNA complex contains the entire closed helix of $mRNA_{L1}$ of *M. jannaschii* and an open helix identical to that of the 38 nt fragment of the TthL1–mRNA complex (Fig. 2*g*). In the MjaL1–mRNA crystal, there are two types of RNA–RNA contacts. One of them is formed by stacking interactions of open and closed ends of RNA molecules, while the other one involves their central parts. The second type of RNA–RNA contacts play a crucial role in the MjaL1–mRNA crystal packing (Fig. 7*a*). Strikingly, this contact involves the same mRNA region that was used for RNA–protein contacts in both types of TthL1–mRNA crystal. Two MjaL1–mRNA complexes related by a noncrystallographic dual axis form a tight dimer strongly stabilized by several hydrogen bonds and three stacking interactions between bulged nucleotides of mRNA fragments. In the MjaL1–mRNA complex RNA helix 2 is 11 nucleotides longer than that in the TthL1–mRNA complex and contains an additional bulged nucleotide. It is possible that the tendency of such nucleotides to form stacking interactions with a neighbouring RNA fragment results in RNA–RNA contacts in the MjaL1–mRNA crystal instead of the RNA–protein contacts found in the TthL1–mRNA crystals.

Two NCS-related tight dimers of MjaL1–mRNA complexes form head-to-tail RNA–RNA contacts in which open and closed ends of RNA molecules interact with each other, in

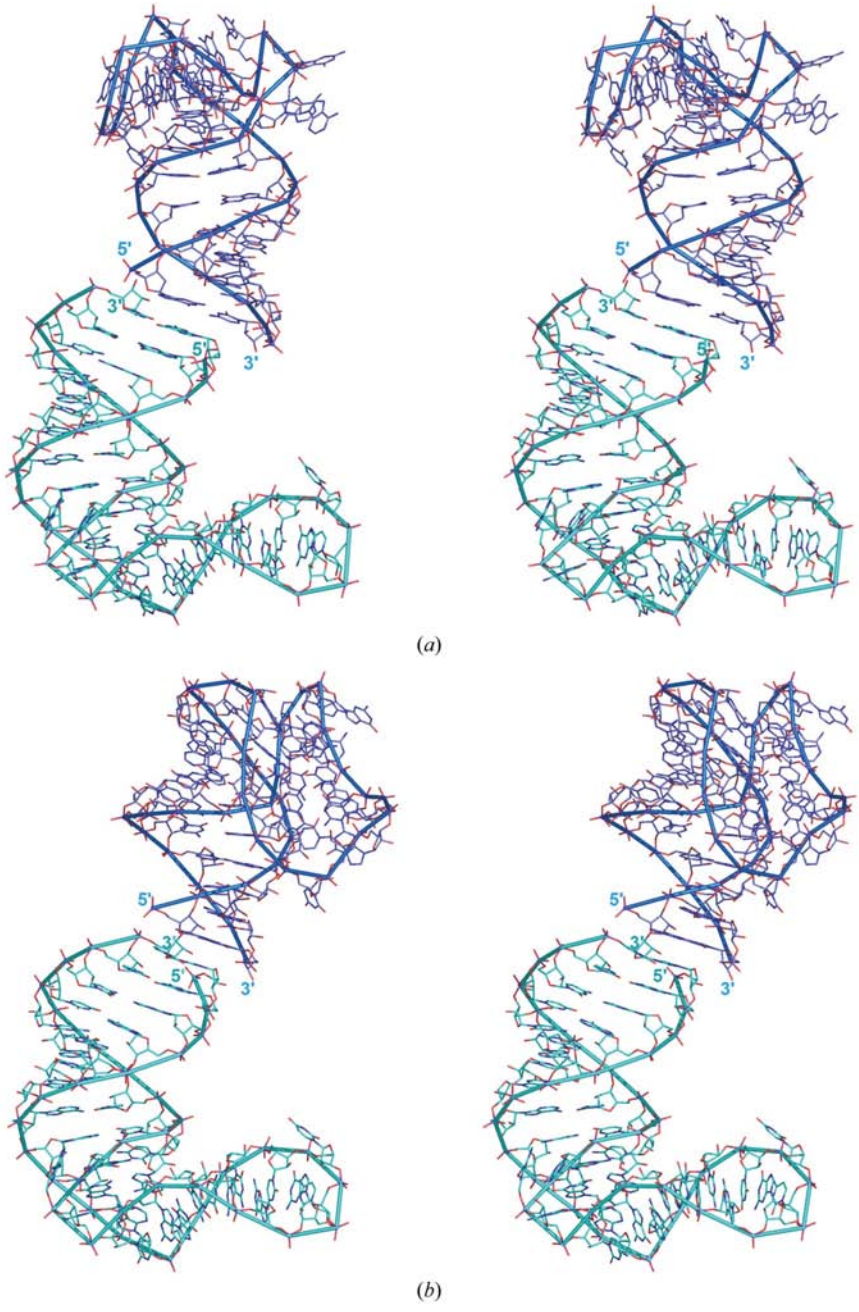

Figure 6
In TthL1–mRNA crystals, interlayer contacts are formed through the open ends of RNA molecules and produce RNA fragments of double length. (*a*) In TthL1–36 nt mRNA, short helices of adjacent RNA molecules are practically perpendicular to each other; (*b*) in TthL1–38 nt mRNA, additional base pairs induce the rotation of short RNA helices of adjacent complexes by about 90°.

contrast to the interaction between open ends in the TthL1–mRNA crystals. This head-to-tail interaction between coaxial helices is strong enough to destroy the terminal G–C canonical base pair at the open end of helix 1 and to stack unpaired guanine with adenine from the closed end of an adjacent RNA molecule. These RNA–RNA contacts produce a flat layer composed of crosscut rows of helices with an angle of about 60° between them.

Adjacent layers interact with each other through weak protein–protein contacts. These contacts are formed by twofold symmetry-related molecules and include helix α2 and loop β6–α7 of the MjaL1 domain II. Such weak interlayer contacts are probably responsible for the low-resolution diffraction patterns of these crystals.

3.5.4. The SacL1–55 nt rRNA complex crystal. Similar to the present complex, SacL1 complexed with a specific fragment of ribosomal RNA from *T. thermophilus* crystallizes in space group $P6_522$ (Nikulin *et al.*, 2003). In SacL1–rRNA crystals, there are also two types of RNA–RNA contacts: between central parts of RNA fragments and between open ends of RNA helices. Interactions through the central parts of RNA fragments differ in MjaL1–mRNA and SacL1–rRNA crystals, but in both cases they produce tight dimers which probably exist in solution. In SacL1–rRNA crystals, twofold symmetry-related complexes form dimers stabilized by two intermolecular canonical base pairs and several hydrogen bonds (Fig. 7*b*). Both oppositely directed open ends of these dimers participate in RNA–RNA stacking interactions, resulting in double extension of helix 1. This produces an infinite superhelix parallel to the *c* axis of the crystal. The superhelix has six complexes per turn and is stabilized by protein–protein interactions formed by twofold symmetry-related loops β6–α6 of the SacL1 domain II. The stacking interactions between open ends of rRNA fragments are similar to those observed in TthL1–mRNA crystals, but in this case both shallow and deep grooves of double-length helix are close to the canonical A-helix.

Weak RNA–protein interactions provide contacts between superhelices in the crystal. These contacts include both loops of the 23S rRNA fragment and helices α3 and α5 of SacL1 domain II.

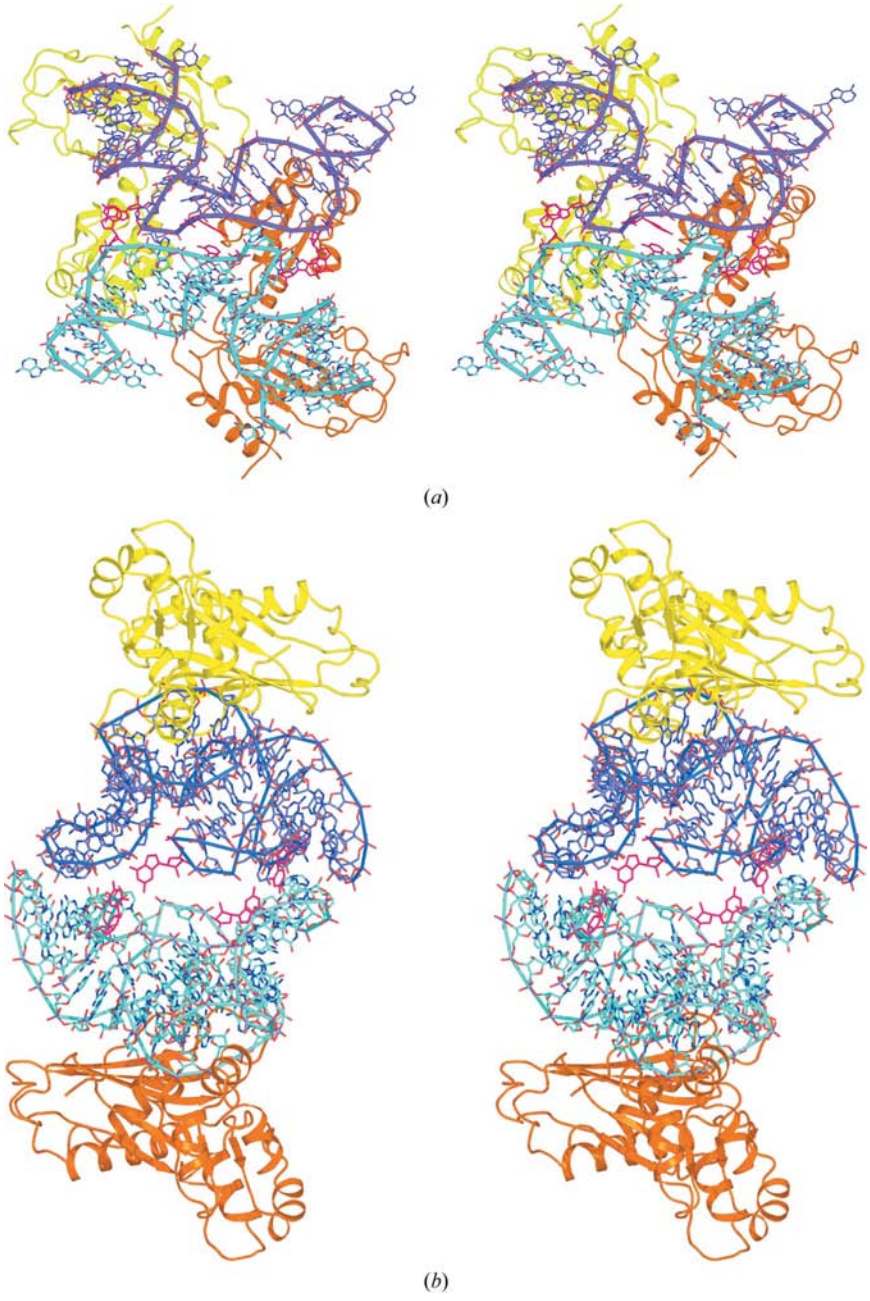

Figure 7
Interaction of adjacent complexes through the central parts of RNA molecules. L1 is shown in yellow or gold and RNA in blue or cyan. Nucleotides involved in intermolecular stacking in the MjaL1–mRNA crystal (*a*) or intermolecular canonical base pairs in the SacL1–rRNA crystal (*b*) are shown in magenta.

3.6. Role of RNA–RNA contacts in crystal formation

Analysis of the crystal packing of known L1–RNA complexes and of RNA–protein complexes formed by ribosomal proteins L11 (Wimberly *et al.*, 1999; Conn *et al.*, 1999), L25 (Lu & Steitz, 2000), S15 (Nikulin *et al.*, 2000), TL5 (Fedorov *et al.*, 2001), L5 (Perederina *et al.*, 2002) and S8 (Tishchenko *et al.*, 2001; Merianos *et al.*, 2004) shows that extension of RNA helices is a common feature of these crystals. Such an extension is induced by stacking interactions between open–open or open–closed ends of RNA fragments. The contact between open ends forms a relatively undistorted extended helix of double length. As can be seen from

a comparison of the crystal packing of the two L1–mRNA complexes, the additional base pair at the open end of the RNA helix induces the mutual rotation of contacting RNA molecules in the crystal by about 90°. The ribosomal proteins specifically bound to these RNA molecules must also change their mutual positions. As a result, a crystal dimer with a new shape is formed. Thus, an alteration of the length of the RNA helices with the open ends is a powerful tool for obtaining new crystal forms of RNA–protein complexes.

Contacts between the open and closed ends of RNA fragments were only found in MjaL1–mRNA crystals. It is possible that such contacts are induced by strong interactions between the central parts of the mRNA fragments and the formation of the cruciate RNA structure.

In most of the known crystal structures of ribosomal proteins specifically bound to corresponding RNAs, complexes contact each other through the central parts of their RNA fragments containing bulged nucleotides. Such contacts are often very extensive and strong and it is possible that they are formed in saturated solution prior to crystal formation. The location of such contact regions on the RNA surface depends on its structure and could be predicted if an RNA structure is known. It is as well to bear in mind that in most cases contacting regions are related by a twofold symmetry axis.

Protein–RNA and protein–protein contacts are different in all known crystals of complexes between ribosomal proteins and RNA. It is likely that in most cases they depend on the structure of the dimers induced by strong RNA–RNA interactions. To improve the quality of crystals, the most suitable contacts can be obtained by using different hybrid complexes between RNA and proteins from different sources.

Similar RNA–RNA contacts, increasing the length of helical regions or forming dimers through bulged nucleotides, are an inherent feature of ribosomal 16S and 23S RNAs (Wimberly *et al.*, 2000; Ban *et al.*, 2000). It is possible to propose that the folding of ribosomal RNAs and the crystallization of RNA–protein complexes are similar processes and the same regions of RNA helices are responsible for formation of contacts in both cases. This enables us to predict functionally important sites on RNA and construct optimal RNA fragments for the purpose of crystallization.

We thank Professor R. A. Zimmermann for critical reading of the manuscript. The research was supported by the Russian Academy of Sciences (RAS), the Russian Foundation for Basic Research (Nos. 04-04-49634 and 05-04-48338), the Program of the RAS on Molecular and Cellular Biology, the Program of the RF President on the support of outstanding scientific schools and the Austrian Science Fund (FWF, P17164-B10). The research of MG was supported in part by an International Research Scholar's award from the Howard Hughes Medical Institute and that of AN by INTAS grant YSF 04-83-3842.

References

Baier, G., Hohenwarter, O., Hofbauer, C., Hummel, H., Stöffler-Meilicke, M. & Stöffler, G. (1989). *Syst. Appl. Microbiol.* **12**, 119–126.

Baier, G., Piendl, W., Redl, B. & Stöffler, G. (1990). *Nucleic Acids Res.* **18**, 710–724.

Ban, N., Nissen, P., Hansen, J., Moore, P. B. & Steitz, T. A. (2000). *Science*, **289**, 905–920.

Brünger, A. T., Adams, P. D., Clore, G. M., DeLano, W. L., Gros, P., Grosse-Kunstleve, R. W., Jiang, J.-S., Kuszewski, J., Nilges, M., Pannu, N. S., Read, R. J., Rice, L. M., Simonson, T. & Warren, G. L. (1998). *Acta Cryst.* D**54**, 905–921.

Conn, G. L., Draper, D. E., Lattman, E. E. & Gittis, A. G. (1999). *Science*, **284**, 1171–1174.

Ennifar, E., Nikulin, A., Tishchenko, S., Serganov, A., Nevskaya, N., Garber, M., Ehresmann, B., Ehresmann, C., Nikonov, S. & Dumas, P. (2000). *J. Mol. Biol.* **304**, 35–42.

Fedorov, R., Meshcheryakov, V., Gongadze, G., Fomenkova, N., Nevskaya, N., Selmer, M., Laurberg, M., Kristensen, O., Al-Karadaghi, S., Liljas, A., Garber, M. & Nikonov, S. (2001). *Acta Cryst.* D**57**, 968–976.

Garber, M., Gongadze, G., Meshcheryakov, V., Nikonov, O., Nikulin, A., Perederina, A., Piendl, W., Serganov, A. & Tishchenko, S. (2002). *Acta Cryst.* D**58**, 1664–1669.

Gongadze, G. M., Korepanov, A. P., Stolboushkina, E. A., Zelinskaya, N. V., Korobeinikova, A. V., Ruzanov, M. V., Eliseev, B. D., Nikonov, O. S., Nikonov, S. V., Garber, M. B. & Lim, V. I. (2005). *J. Biol. Chem.* **280**, 16151–16156.

Gourse, R. L., Sharrock, R. A. & Nomura, M. (1986). *Structure, Functionand Genetics of Ribosomes*, edited by B. Hardesty & G. Kramer, pp. 766–788. New York: Springer–Verlag.

Gourse, R. L., Thurlow, D. L., Gerbi, S. A. & Zimmermann, R. A. (1981). *Proc. Natl Acad. Sci. USA*, **78**, 2722–2726.

Hanner, M., Mayer, C., Köhrer, C., Golderer, G., Grobner, P. & Piendl, W. (1994). *J. Bacteriol.* **176**, 409–418.

Jones, T. A., Zou, J.-Y., Cowan, S. W. & Kjeldgaard, M. (1991). *Acta Cryst.* A**47**, 110–119.

Kabsch, W. (2001). *International Tables for Crystallography*, Vol. *F*, edited by M. G. Rossmann & E. Arnold, pp. 218–225. Dordrecht: Kluwer Academic Publishers.

Köhrer, C., Mayer, C., Neumair, O., Gröbner, P. & Piendl, W. (1998). *Eur. J. Biochem.* **256,** 97–105.

Kraft, A., Lutz, C., Lingenhel, A., Gröbner, P. & Piendl, W. (1999). *Genetics*, **152**, 1363–1372.

Leontis, N. B. & Westhof, E. (2001). *RNA*, **7**, 499–512.

Lim, V. I. & Garber, M. B. (2005). *J. Mol. Biol.* **346**, 395–398.

Lu, M. & Steitz, T. A. (2000). *Proc. Natl Acad. Sci. USA*, **97**, 2023–2028.

Mayer, C., Köhrer, C., Gröbner, P. & Piendl, W. (1998). *Mol. Microbiol.* **27**, 455–468.

Merianos, H. J., Wang, J. & Moore, P. B. (2004). *RNA*, **10**, 954–964.

Navaza, J. (1994). *Acta Cryst.* A**50**, 157–163.

Nevskaya, N. A., Nikonov, O. S., Revtovich, S. V., Garber, M. B. & Nikonov, S. V. (2004). *Mol. Biol. (Moscow)*, **38**, 789–798.

Nevskaya, N., Tishchenko, S., Gabdoulkhakov, A., Nikonova, E., Nikonov, O., Nikulin, A., Platonova, O., Garber, M., Nikonov, S. & Piendl, W. (2005). *Nucleic Acids Res.* **33**, 478–485.

Nevskaya, N., Tishchenko, S., Volchkov, S., Kljashtorny, V., Nikonova, E., Nikonov, O., Nikulin, A., Köhrer, C., Piendl, W., Zimmermann, R., Stockley, P., Garber, M. & Nikonov, S. (2006). *J. Mol. Biol.* **355**, 747–759.

Nikonov, S., Nevskaya, N., Eliseikina, I., Fomenkova, N., Nikulin, A., Ossina, N., Garber, M., Jonsson, B.-H., Briand, C., Svensson, A., Aevarsson, A. & Liljas, A. (1996). *EMBO J.* **15**, 1350–1359.

Nikulin, A., Eliseikina, I., Tishchenko, S., Nevskaya, N., Davydova, N., Platonova, O., Piendl, W., Selmer, M., Liljas, A., Drygin, D.,

Zimmermann, R., Garber, M. & Nikonov, S. (2003). *Nature Struct. Biol.* **10**, 104–108.
Nikulin, A., Serganov, A., Ennifar, E., Tishchenko, S., Nevskaya, N., Shepard, W., Portier, C., Garber, M., Ehresmann, B., Ehresmann, C., Nikonov, S. & Dumas, P. (2000). *Nature Struct. Biol.* **7**, 273–277.
Perederina, A., Nevskaya, N., Nikonov, O., Nikulin, A., Dumas, P., Yao, M., Tanaka, I., Garber, M., Gongadze, G. & Nikonov, S. (2002). *RNA*, **8**, 1548–1557.
Tishchenko, S., Nikulin, A., Fomenkova, N., Nevskaya, N., Nikonov, O., Dumas, P., Moine, H., Ehresmann, B., Ehresmann, C., Piendl, W., Lamzin, V., Garber, M. & Nikonov, S. (2001). *J. Mol. Biol.* **311**, 311–324.
Wimberly, B. T., Brodersen, D. E., Clemons, W. M. Jr, Morgan-Warren, R. J., Carter, A. P., Vonrhein, C., Hartsch, T. & Ramakrishnan, V. (2000). *Nature (London)*, **407**, 327–339.
Wimberly, B. T., Guymon, R., McCutcheon, J. P., White, S. W. & Ramakrishnan, V. (1999). *Cell*, **97**, 491–502.